Experience from Laboratory Testing of Commercial Silicon Bonded Silicon Carbide Materials. Typical Properties and Analyses

Egil Skybakmoen[1] and Zhaohui Wang[2]
1. Research Manager
2. Research Scientist
SINTEF Materials and chemistry, Trondheim, Norway
Corresponding author: egil.skybakmoen@sintef.no

Abstract

Silicon nitride bonded silicon carbide is currently the most common type of sidelining material in aluminium electrolysis cells. The material has replaced carbon due to better chemical resistance, better oxidation resistance, and better thermal performance, which opens for increased productivity. Today, many producers offer carbide based sidelining materials, and the users ask for quality evaluations. During the last two decades, SINTEF and partly NTNU have developed test methods and analyses for quality evaluation. The studies have been financed through national research programs as well as by testing of materials from the different suppliers. The work has contributed to improved characterisation and descriptions of the most important material parameters, as well as better understanding of the industrial performance. The present paper describes our findings regarding typical physical and chemical parameters, based on analyses and tests of several hundred samples from suppliers worldwide. The results from some autopsies of industrial cells for studying the degradation mechanisms are included. Based on our findings and experience, a set of up-dated recommendations and useful specifications for suppliers as well as for users has been worked out.

Keywords: Aluminium electrolysis cell, sidelining materials, silicon nitride bonded SiC, test and analysis, specifications

1. Introduction

SINTEF started the research work regarding Nitride bonded sidelining materials in 1995 financed by the Norwegian Aluminium industry (that time Hydro Al, Elkem Al and Søral) and the Research Council of Norway (RCN). The aim was to establish relevant analysis and test methods to be able to check, and qualify, the commercial materials at the market. The main challenge was to develop a realistic test method in laboratory scale for measuring the chemical resistance to simulate the chemical conditions found in industrial cells. The latest 20 years we also developed analysis of other important parameters for quality checks; physical and mechanical properties, thermal properties and mineral phase analysis. An overview over typical results measured will be presented in this paper.

2. Silicon Nitride Bonded SiC

The use of Silicon Nitride bonded SiC refractories as sidelining is today the state of the art in modern high amperage cells. It exists many producers and hence also quality differences on the global market. For the users, it is important to have a stable and reliable quality. It is always also a question what kind of material properties make a good quality and therefore the intention with this paper is to present our main findings based on test work from many suppliers the latest 20 years. Our work and research on this field have regularly been published [1 - 6].

2.1. Production Route

A typical production route for Nitride bonded SiC is shown in Figure 1. As raw materials, SiC grains and Si particles are used together with an organic binder. This is pressed to a green block with desired dimension. The green blocks are going through a drying step before entering the nitridation step in furnaces purged with Nitrogen gas to establish the binder phase Si_3N_4. The finished products then consist of SiC bonded by a phase of Si_3N_4.

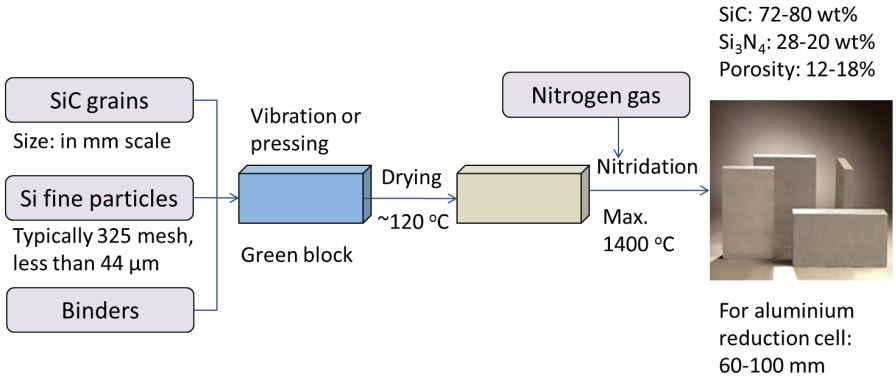

Figure 1. Schematic production route of Nitride bonded SiC.

A Si3N4 bonded SiC brick often consists of 72-80 wt% SiC and 20-28 wt% Si3N4 phases. Figure 2 shows the typical microstructure of the composite material, where coarse SiC grains dispersed in fine nitride binder phase.

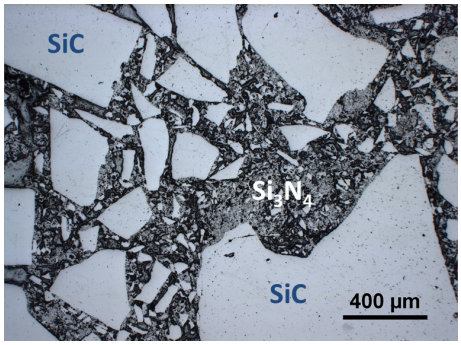

Figure 2. Optical image of a polished Si3N4 bonded SiC brick surface.

The Si_3N_4 binder phase is formed during the nitridation process and often consists of both an α- and a β- phase. The morphology of α- and β-Si_3N_4 phases is shown in Figure 3. The β-Si_3N_4 phase is the thermodynamic stable phase and favored by high temperature and presence of liquid Si or FeSi phase, while α-Si_3N_4 is formed by gaseous phase reactions and often stabilized by oxygen impurities. The nitridation temperature is not sufficient high to fulfill the complete α- to β-Si3N4 phase transition, so a mixture of α- and β-Si_3N_4 is common in this type of composite. The ratio between the two nitride phases varies and is depending on the fabrication conditions including but not limited to particle size of Si powders, temperature, atmosphere composition, impurities in the starting materials and additives [7, 8]. By tuning the fabrication conditions, the α- to β- phase ratio could be to some degree modified.

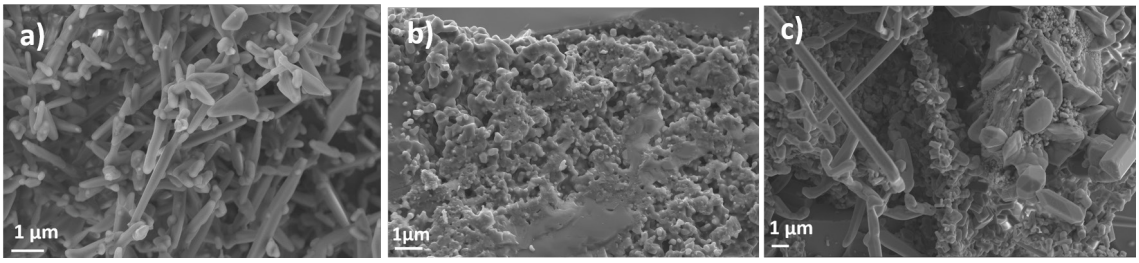

Figure 3. Scanning electron microscopy image for Si_3N_4 binder phase. a) α-Si_3N_4 needles, b) α-Si_3N_4 matte, and c) β-Si_3N_4 rods.

The composite material is however not homogeneous. A higher amount of α- phase at periphery area of a brick and a higher amount of β- phase at the interior area is often observed. This is determined by the nature of the fabrication process. The temperature is actually higher in the interior part of the brick due to the exothermic nitridation reaction of Si powders, while the oxygen potential is diffusion control so it is low in the center part. This favored the β- phase formation. α- phase is often formed at initial state of the nitridation and favored at the surface. Additives in the green block can also significantly changed the α- to β-Si_3N_4 ratio. Bricks with almost only β-Si3N4 as binder phase is thus also available. A schematic drawing is shown in Figure 4 to illustrate the distribution of temperature and oxygen partial pressure distribution along the cross section of a brick.

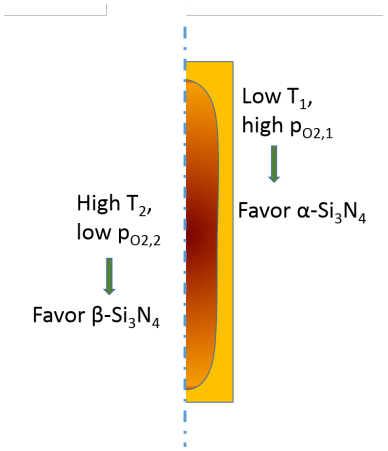

Figure 4. Schematic drawing of fabrication condition showing higher temperature and low oxygen partial pressure at the interior part of the brick.

For a more detailed and theoretically considerations regarding microstructures it refers to papers by Skybakmoen et al from 2014 [5] and recently from Long et al 2016 [6].

2.2. Relevant Test Methods

The most relevant parameters to be tested and analysed are shown in Table 1.

Table 1. Relevant test methods.

Test Parameter	Standard method	# of samples from the block and position
Physical properties:		
Open porosity (%)	ISO 5017	4 (2 outer and 2 inner)
Density (g/cm^3)	ISO 5017	4 (2 outer and 2 inner)
Thermal expansion to 1200 °C (%)	DIN 51045	1
Thermal conductivity to 1000 °C (W/mk)	Laser Flash, NETZSCH LFA 457	2 (outer and inner)
Mechanical properties:		
Cold crushing strength (MPa)	ISO 10059-1	2 (outer and inner)
Bending strength (MPa)	ISO 5014	2 (outer and inner)
Mineralogical / chemistry:		
Total SiC, α-Si_3N_4, β-Si_3N_4, Si_2ON_2, Si (wt%)	XRD Rietveld	2 (outer and inner)
Total oxygen and total nitrogen (wt%)	LECO	2 (outer and inner)
Microstructure:		
Pore size distribution, pore surface area(m^2/g)	Mercury porosimetry	2 (outer and inner)
Structure	SEM and light microscopy	2 (outer and inner)
Special test methods:		
Chemical resistance, polarised 50 h	SINTEF	4 (2 outer and 2 inner)
Oxidation in air at 950 °C for 100 h	SINTEF	2 (outer and inner)

2.3. Sampling Procedures

It was observed early that these kind of materials is not homogenous. For this reasons it is of great importance to define the samples position within the block. Normally, all test and analysis were performed within a 10 mm thick slice cut from the middle of a block, shown in Figure 5 (left frame). A selected number of test methods and their sampling positions are indicted in Figure 5 to the right.

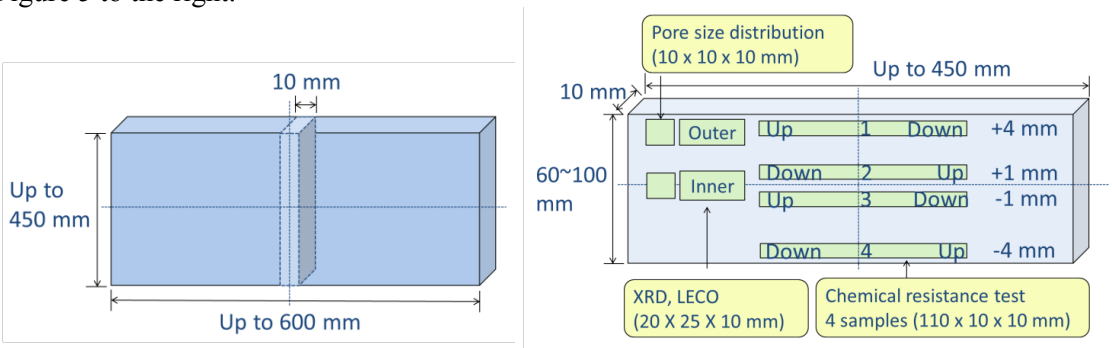

Figure 5. Sampling positions and corresponding test methods (not in scale). "Up" and "Down" denotes the sample positions in the chemical resistance test cell. Drawing to right is the enlarged figure of the slice in the drawing to the left.

2.4. Physical Properties – Open Porosity, Density, Thermal Expansion and Thermal Conductivity

Based on all tests and analysis the latest 20 years it exists a lot of data regarding open porosity and density (more than 550 samples). Thermal expansion and thermal conductivity is measured on fewer samples (around 20 samples). An overview over the results is shown in Table 2.

Table 2. Overview typical physical properties measured.

Test parameter	Max	Min	AVG/STDEV	# samples
Open porosity (%)	20.45	11.20	15.52 ± 1.70	558
Density (g/cm^3)	2.86	2.51	2.68 ± 0.06	558
Thermal exp. to 1200 °C (%)	0.54	0.47	0.50 ± 0.02	17
Coeff. of linear expansion (10^{-6} /K)	4.70	4.00	4.33 ± 0.19	17
Thermal conductivity (W/mK)				
Room temperature	50	24	35.6 ± 6.7	20
750 °C	23	10	18.8 ± 2.8	20

It is often observed a variation in porosity (and density) within the block positions. Some examples is shown in Figure 6. The variations may be very different from block to block, but in general the variations are larger with increased thickness of the block.

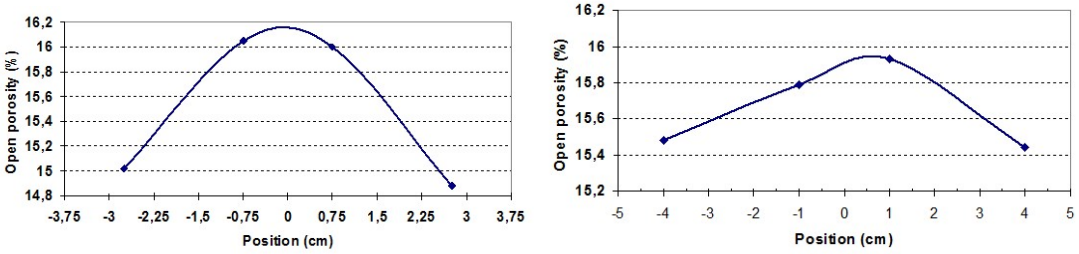

Figure 6. Variations in porosity within the block thickness (0 is middle in the block).

In general, the thermal expansion is similar for all the blocks tested. A typical example is shown in Figure 7.

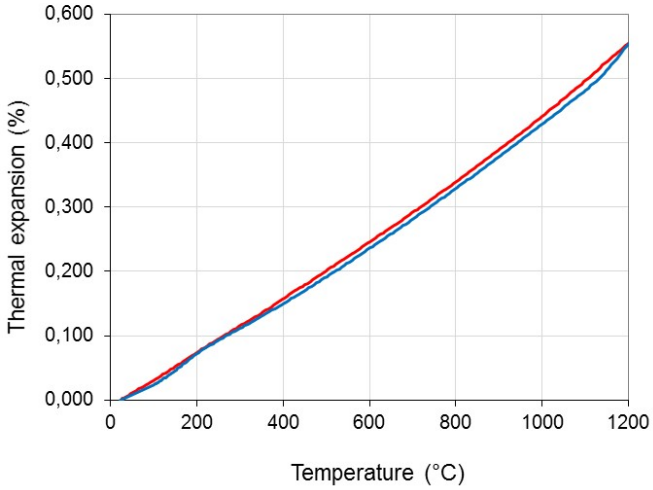

Figure 7. Thermal expansion up to 1200 °C.

Thermal conductivity is an important parameter for sidelining materials and we do use the Laser Flash method from RT up to 900 °C. A typical measurement is shown in Figure 8.

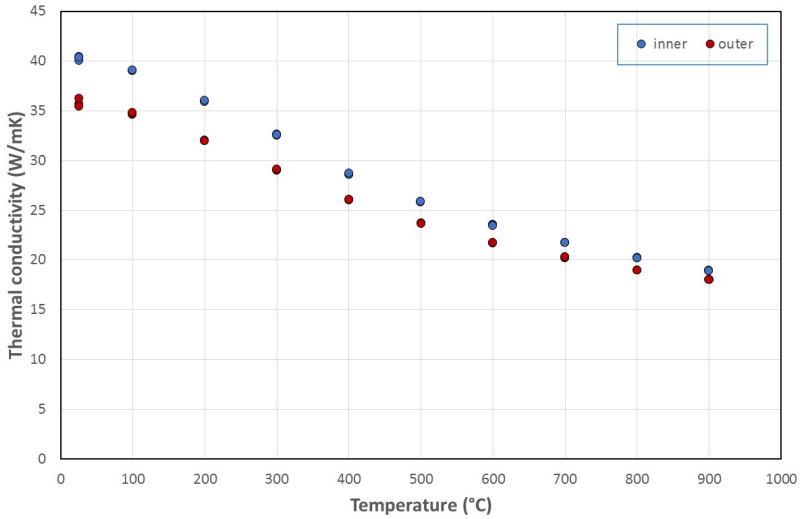

Figure 8. Thermal conductivity from RT to 900 °C. Inner and outer samples.

2.5. Mineral Phase Analysis (XRD) and Total Oxygen and Total Nitrogen (LECO)

The mineral phase composition was measured by LECO and XRD analysis. The samples were crushed to a fine powder (-100 µm) in a tungsten carbide mortar. The sample for XRD was further milled down to 45 µm.

Powder X-ray diffraction (XRD) data were collected on a Bruker AXS D8 Focus diffractometer with a Lynxeye^{TM} detector using CuKα radiation accelerated at 40 kV and 40 mA, scanning in the 2θ range from 10° to 80° with a step size of 0.016°. Scans were collected with counting times between 0.25 and 1.4 seconds per step. The XRD data were refined using Bruker AXS' Topas v4.2 Rietveld refinement software. The background was modelled using a Chebychev polynomial, and a Fundamental Parameter peak shape was used to describe the Bragg reflections

The total oxygen and nitrogen content was determined by using a LECO TC436DR (LECO Corporation, USA). The analysis was performed by heating a small amount of the sample (in a tin capsule) together with graphite powder to a temperature high enough for the oxides to react with carbon and form CO and CO_2, and the nitrides to decompose giving free nitrogen. The CO (g) and CO_2 (g) formed were detected by IR absorption and the nitrogen content is detected by thermal conductivity. The samples were analysed at a temperature of approximately 2750 °C. Helium 6.0 was used as a carrier gas. The instrument was calibrated twice per day using standard steel samples (0.0363 ± 0.0006 wt% oxygen, 0.172 ± 0.0032 wt% nitrogen).

Normally samples from outer and inner part were analysed from the blocks (as shown in Figure 5).

An overview of all the results obtained is given in Table 3.

Table 3. Overview mineral phase analysis (XRD) and total oxygen and nitrogen (LECO). Inner and outer samples.

Parameter	Range		Average ± standard deviation		# samples
	Inner	Outer	Inner	Outer	
SiC	73.7 - 84.2	73.1 - 83.2	79.3 ± 2.4	77.3 ± 2.5	37
α-Si_3N_4	2 - 19.6	4.8 - 25.3	8.54 ± 4.79	13.8 ± 5.4	37
β-Si_3N_4	0.9 - 17.9	0.6 – 17.7	8.4 ± 4.0	7.0 ± 4.8	37
Ratio α/β	0.13 - 13.33	0.3 - 42.17	1.94 ± 2.71	5.17 ± 8.02	37
Si_2ON_2	0 - 9.5	0 - 8.4	2.3 ± 2.4	1.2 ± 2.0	37
Si	0.09 - 6.6	0.04 - 2.4	0.92 ± 1.5	0.3 ± 0.4	37
Total O	0.36 – 2.12	0.33 – 1.75	0.84 ± 0.44	0.74 ± 0.35	37
Total N	0.6 – 10.3	1.0 – 11.7	7.8 ± 1.8	8.7 ± 1.7	37

2.6. Mechanical Properties

As long the materials have small amounts of free Si (well nitridated) the mechanical properties are very good. If the materials are broken through installations in the cells it may be due to bad nitridation during the production process.

Typical values of cold crushing strength and bending strength are shown in Table 4 based on our tests from a number of various materials.

Table 4. Measured values CCS and bending strength.

Parameter	Max	Min	Average ± standard deviation	# samples
CCS (MPa)	401	123.8	248.8 ± 65.4	82
Bending strength (MPa)	72.2	20.5	45.2 ± 12.2	61

2.7. Oxidation Resistance in Air at 950 °C

The oxidation test was performed by suspending the sample (dimension 60 x 30 x 15 mm) from a balance in a resistance heated tube furnace. The furnace was heated at a rate of 300°C/h to 950°C and then kept at 950°C for 100 hours. A constant flow of 50 ml/s of synthetic air was maintained through the furnace throughout the entire test. The course of oxidation in terms of weight change of the sample was recorded continuously during the test. The weight change is also registered by weight before and after the test. A typical weight increase by time is shown in Figure 9.

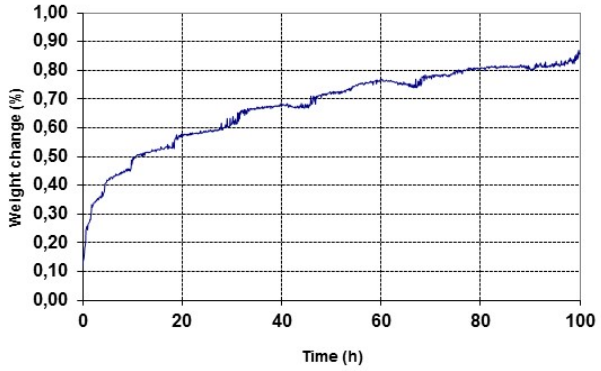

Figure 9. Typical weight increase in air at 950 °C for 100 h.

However, we do observe sometimes weight decrease during heat-up to 950 °C, normally observed at temperature 550 – 600 °C. This observation indicates some free C to react with the present air. One example with this observation is shown in Figure 10.

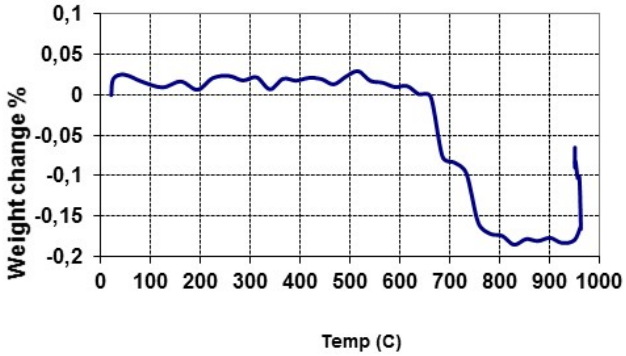

Figure 10. Weight decrease during heat-up in air.

An overview over typical weight increases after 100 h at 950 °C is between 0.04 – 1.15 wt % and with average 0.66 ± 0.29. (34 samples).

2.8. Chemical Resistance Test Method

It exists several methods to measure and test the chemical resistance of these kind of materials however no standard test method exists. SINTEF started to evaluate several possibilities in middle of the 1990's and after 2 - 3 years of development work we ended up with a 50 h polarised test method. The main aim of the test set-up was to simulate the chemical conditions found in industrial environments and also to be able to make a quality ranking of commercial materials. The test method is suitable to improve materials quality and also to increase the understanding of the degradation mechanism taken place in industrial cells.

The test cell set-up is shown in Figure 11. The initial composition of the bath at the start of the electrolysis was 10 wt% AlF_3 in excess, 5 wt% CaF_2, 7 wt% Al_2O_3 and balance Na_3AlF_6. The temperature was 955 ± 2 °C. The test time is 50 h. After 25 h the anode was changed and 25 g cryolite and 5 g alumina were added. The anode consumption was measured by weight.

After the test, the crucible with the test pieces was cooled for about 12 hours. The graphite lid was removed, and the rest of the test cell was heated up again in an open furnace, and the test pieces were removed from the crucible as soon as the bath melted. Adhering bath was removed mechanically and by washing in an aqueous solution of $AlCl_3$.

The degree of degradation is assessed by the volume loss of the pieces during the test. The volume of the test materials was measured before and after the test by using ISO 5017 standard.

The volume loss of each piece was estimated (volume before – volume after) and a scale describing the degree of degradation was made with a scale from 0 - 10 where 0 is the best and 10 is the worst.

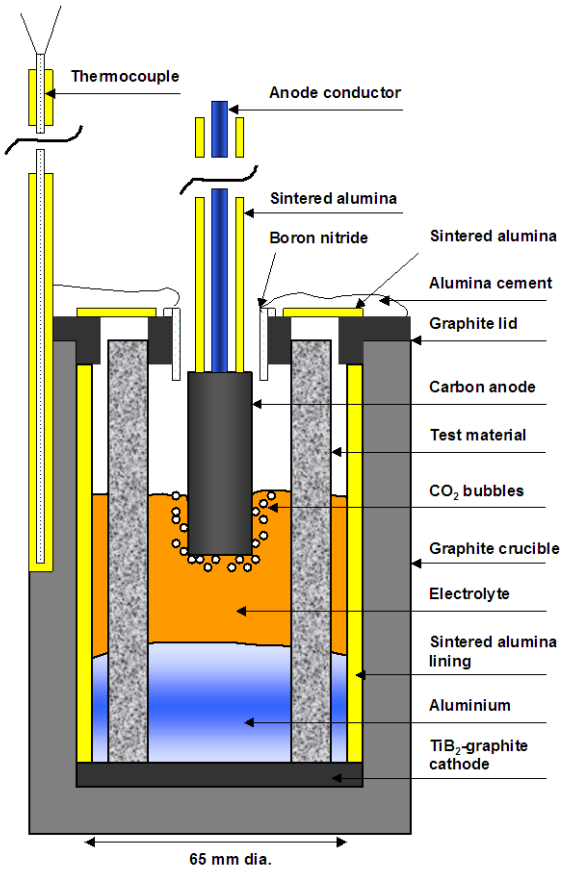

Figure 11. Chemical resistance test cell set-up.

Normally it is tested 4 samples from the same block (defined positions within the block). This gives an average level of degradation of 4 samples from the same block. However, we also can test samples from different blocks in the same test.

The materials tested normally undergo degradation in the gas phase zone (zone above the bath) much like observations from industrial cells. Strongly degraded samples even showed visible degradation in the upper bath level zone. In some cases, the test samples are completely degraded in the gas phase zone. In Figure 12 is shown a picture of samples after the test. In this case, “good” and “poor” quality samples where tested in two different tests.

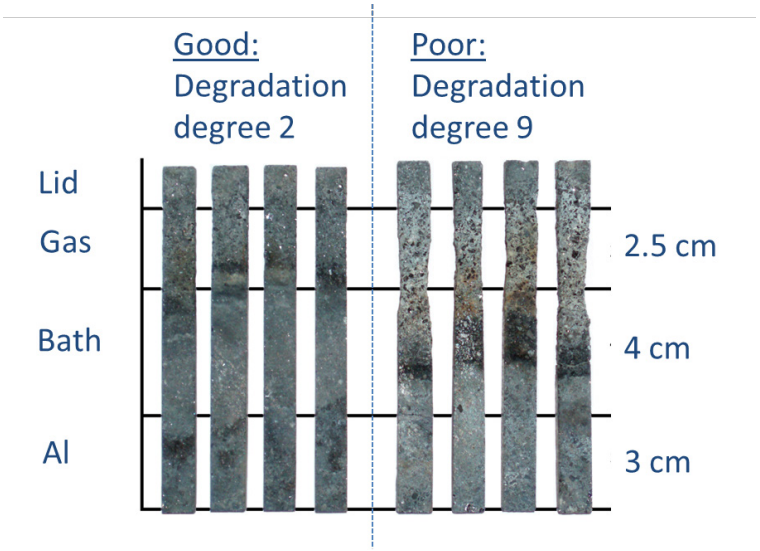

Figure 12. Typical samples after the test. Good (degradation 2) and bad (degradation 9) quality materials.

Since 1996 about 550 samples delivered by about 20 suppliers/plants have been tested. The volume loss of the samples have varied between 0.07 – 20.65 % with an average value of 5.05 ± 3.33 %, which corresponds to an average degree of degradation equal to 6. The distribution regarding the degree of degradation of all the tests is shown in Figure 13. It means around 31% shown degree of degradation from 0 - 3, from 4 - 7 it is 45 % while around 24% of all samples tested have degree of degradation from 8 - 10. In my opinion it is most important to avoid the really high degraded qualities above 8. Whether it is 3 or 7 may have less impact in industrial cells.

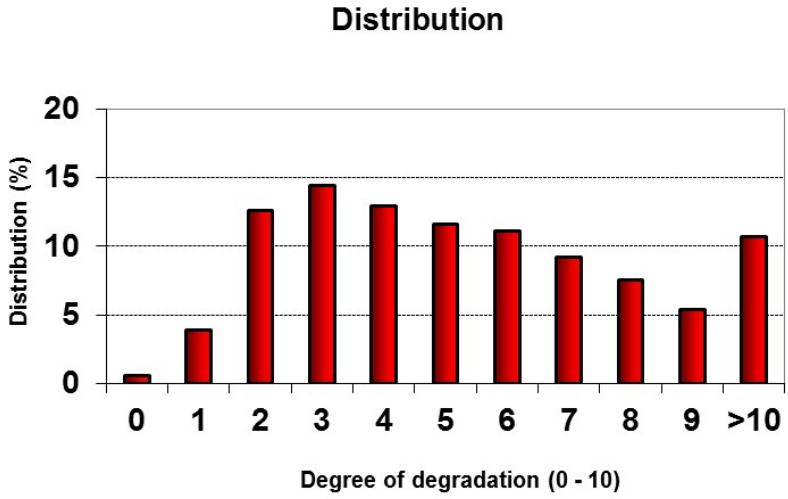

Figure 13. Distribution of the degree of degradation based on 550 samples.

3. Typical variations across the blocks

Since the samples analysed is taken systematic from different positions within the blocks tested it was registered some typical variations between inner and outer parts of the blocks. Some general variations is listed in Table 5.

Table 5. Typical variations between inner and outer part of the block.

Properties	Peripheral part	Central part
Apparent porosity	Lower	Higher
Density	Higher	Lower
Free Si	Lower	Higher
Alpha-Si_3N_4	Higher	Lower
Beta-Si_3N_4	Lower	Higher
Total oxygen	Lower	Higher
Si_2ON_2	Lower	Higher
Pore surface area	Higher	Lower
Chemical resistance	Lower	Higher

4. Comparison Between Two Commercial Blocks

In order to investigate the importance of the different properties we did a study between 2 different commercial materials – here noted as material A and material D. The following analysis were performed: Porosity and density, mineral phase analysis (XRD and LECO), pore size distribution, oxidation resistance in air at 950 °C for 100 h and chemical resistance test 50 hours polarised test.

The porosity and density was the same for the blocks, while it was detected differences in mineral phase compositions as well as pore size distribution (Mercury porosimeter, Micromeritics AutoPore IV 9500 Series), oxidation resistance and chemical resistance.

The pore size distribution is shown for block A and block D in Figure 14.

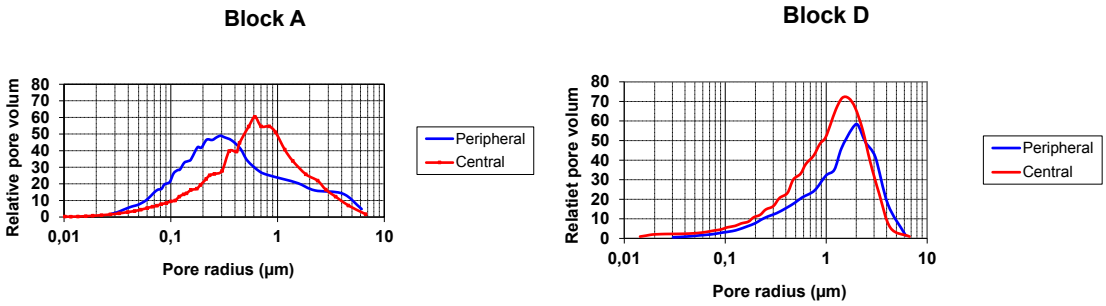

Figure 14. Pore size distribution Block A and Block D – central and peripheral part.

For Block A the pores are much smaller than Block D and thus also higher pore surface area.

The oxidation in air at 950 °C for 100 h also showed large differences as shown in Figure 15.

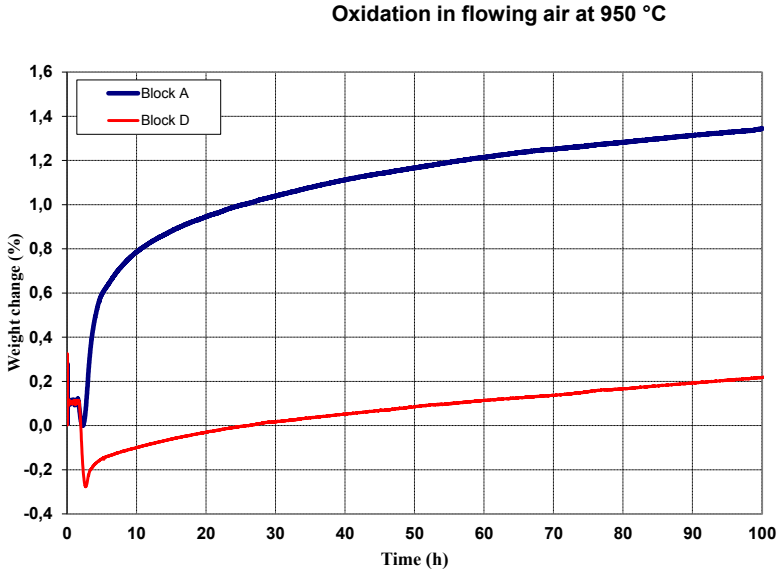

Figure 15. Oxidation in air at 950 °C for 100 h. Block A and Block D.

All results are summarized in Table 6.

Table 6. Comparisons results Block A and Block D.

Properties	A Outer	A Inner	D Outer	D Inner
Porosity (%)	15.68	15.98	16.27	16.33
Density (g/cm^3)	2.69	2.67	2.66	2.66
Total O (wt%)	1.61	2.12	0.63	0.62
Total N (wt %)	9,75	9.08	11.68	10.22
SiC (wt %)	76,8	78.8	76.1	77.4
α-Si_3N_4	18	12	19	13
β-Si_3N_4	0,9	0.9	4.9	10
Ratio α / β	20	13.3	3.9	1.3
Si_2ON_2	4	5.9	0	0.4
Si	0.2	0.1	0.1	0.1
Pore surface area (m^2/g)	0.47	0.32	0.12	0.27
Oxidation weight increase (%)	1.31	-	0.19	-
Chemical resistance (vol %)[1]	Avg 12.62	12.91	1.41	Avg 4.38
Chemical resistance (scale 0-10)	10	10	2	5

[1] Chemical resistance test: 2 samples A outer and D Inner. Average values in shown in Table 5.

The results in this comparison test between the 2 blocks is clear: Low total oxygen, low ratio α/β ratio, low Si_2ON_2, low pore surface area and low oxidation weight increase gives the best chemical resistance.

5. Industrial Relevance

In industrial cells it is often observed degradation in the gas phase zone above the electrolyte level as like in the laboratory test cell set-up. Previous studies by Wang et al [9, 10, 11] based on several autopsies from industrial cells concluding the degradation mechanism is different in the upper and lower part of the sidelining due to the different chemical environments. In the upper part it is selective oxidation by oxidizing gases and HF/$NaAlF_4$ gases resulting in formations of Si_2ON_2 and SiO_2 and SiC grains detachment. This is illustrated in Figure 16.

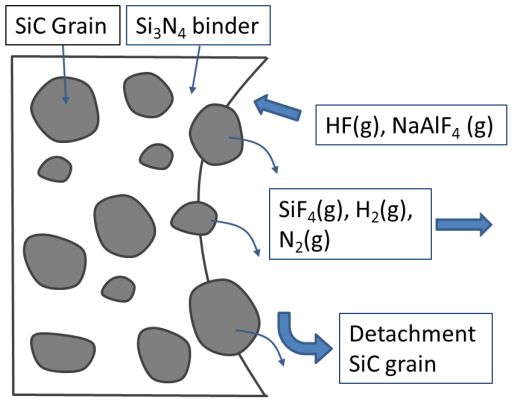

Figure 16. Degradation mechanism in the top part of the block surface.

In the lower level it is obtained infiltration by Na and formation of Na_2SiO_3. The material is densified but thermal conductivity is decreased up to 50 %. A schematic overview of the degradation mechanism is shown in Figure 17.

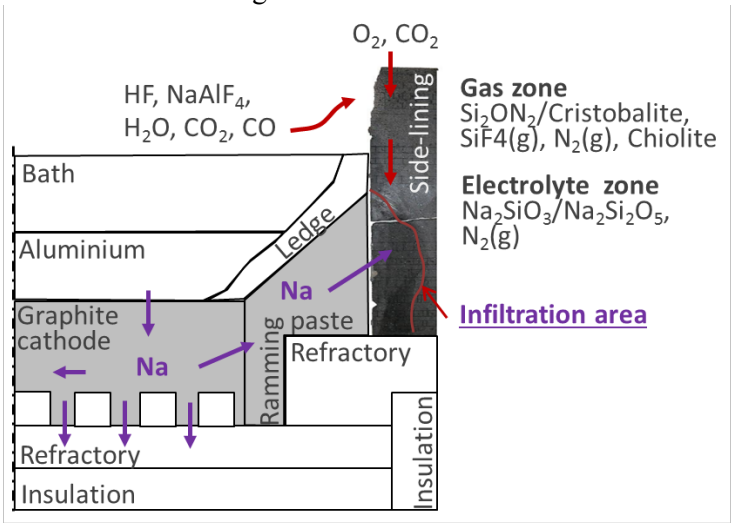

Figure 17. Schematic overview of degradation mechanism of sidelining materials.

When the side ledge is unstable the degradation will occur and hence the best protection will be stable operation conditions.

When it comes to specifications of the best Nitride bonded SiC material we would recommend the following:

1. Define the samples positions for test and analysis. The blocks are inhomogeneous.
2. Be sure it is stable quality each single block with well nitridation (free Si < 0.5 wt%).
3. Lowest total oxygen content and oxide compounds.
4. The microstructure should give low pore surface area as possible.
5. Avoid materials with high degree of degradation in the chemical resistance test (above 8 on our scale).

It is obvious that all blocks are inhomogeneous with respect to the content of α-Si_3N_4 and β-Si_3N_4 due to reaction mechanisms in the production routes. If it is possible to control, it seems the ratio α/β-Si_3N_4 should be as low as possible.

It should also be mentioned that laboratory tests will give in-put to improvements and more understanding of all parameters involved to optimize the required properties. However, it will always be some uncertainty in analysis and tests also in laboratories with respect to reproducibility and test methods itself.

6. References

1. E. Skybakmoen, H. Gudbrandsen and L.I. Stoen, Chemical resistance of sidelining materials based on SiC and carbon in cryolitic melts – a laboratory study, *Light Metals* 1999, 215-222.
2. E. Skybakmoen, Evaluation of chemical resistance/oxidation of Si_3N_4-SiC sidelining materials used in Al electrolysis cells, *Proceedings of Unified International Technical Conference on Refractories*, Volume III, 1330 – 1339, Cancun, Mexico, Nov 2001.
3. E. Skybakmoen, L. I. Støen, J. H. Kvello and O. Darell, Quality evaluation of nitride bonded silicon carbide sidelining materials, *Light Metals* 2005, 773-778.
4. E.Skybakmoen, J.H. Kvello, O.Darell and H. Gudbrandsen, Test and analysis of nitride bonded SiC sidelining materials. Typical properties analysed 1997-2007, *Light Metals* 2008, 943-948.
5. E. Skybakmoen, Z.Wang, T.Grande, The influence of microstructure of Si_3N_4-SiC side-lining materials on chemical/oxidation resistance behaviour tested in laboratory scale, *11th Australasian Aluminium Smelting Technology Cconference*, Dubai, 6 - 11 December 2014.
6. M. Long, Y.Li, H.Qin,W.Xue, J.Chen, J. Sun, R.V. Kumar, Formation mechanism of Si_3N_4 in reaction-bonded Si_3N_4-SiC composites, Ceramics International, 42 (2016) 16448-16452.
7. A.J.Moulsen, Reaction-bonded silicon nitride:It's formation and properties, *J.Mater.Sci*., 14 (1979), 1017-1051.
8. G.Ziegler, J.Heinrich, G.Wötting, Relationships between processing, microstructure and properties of dense and reaction-bonded silicon nitride, *J.Mater.Sci.*, 22 (1987) 3041-3086.
9. Z. Wang, Aging of Si_3N_3-bonded SiC sidewall materials in Hall-heroult cells, *PhD thesis*, 2010, Norwegian University of Science and Techonology: Trondheim.
10. Z. Wang, E. Skybakmoen, and T. Grande, Chemical Degradation of Si_3N_4-Bonded SiC Sidelining Materials in Aluminum Electrolysis Cells. *Journal of the American Ceramic Society*, 2009, 92(6), 1296-1302.
11. Z. Wang, E. Skybakmoen, and T. Grande, Thermal Conductivity of Porous Si_3N_4-Bonded SiC Sidewall Materials in Aluminum Electrolysis Cells, *Journal of the American Ceramic Society*, 2012. 95 (2), 730-738.